SUPPLEMENT

EXPLAINING EXTREME EVENTS OF 2016 FROM A CLIMATE PERSPECTIVE

Editors
Stephanie C. Herring, Nikolaos Christidis, Andrew Hoell, James P. Kossin,
Carl J. Schreck III, and Peter A. Stott

Special Electronic Supplement to the
Bulletin of the American Meteorological Society
Vol. 99, No. 1, January 2018

Cover credits:
©The Ocean Agency / XL Catlin Seaview Survey / Chrisophe Bailhache—A panoramic image of coral bleaching at Lizard Island on the Great Barrier Reef, captured by The Ocean Agency / XL Catlin Seaview Survey / Christophe Bailhache in March 2016.

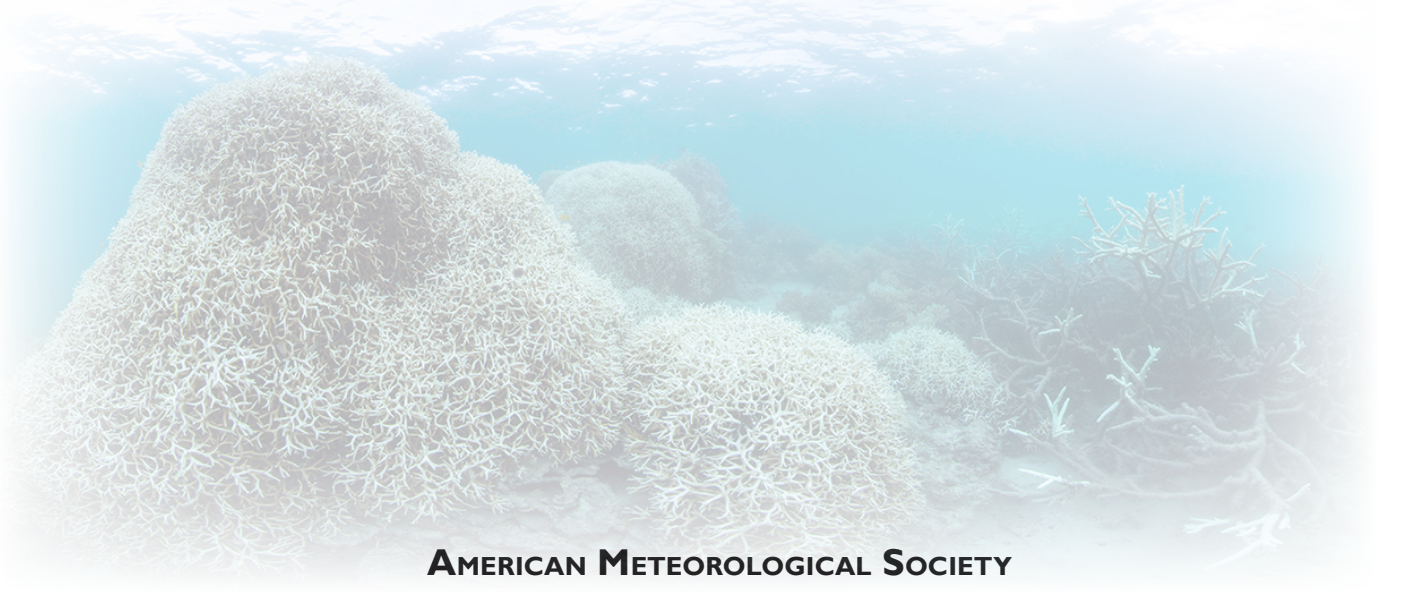

AMERICAN METEOROLOGICAL SOCIETY

ES9. ANTHROPOGENIC AND NATURAL INFLUENCESON RECORD 2016 MARINE HEATWAVES

Eric C. J. Oliver, Sarah E. Perkins-Kirkpatrick, Neil J. Holbrook and Nathan L. Bindoff

This document is a supplement to "Anthropogenic and natural influences on record 2016 marine heatwaves," by Eric C. J. Oliver, Sarah E. Perkins-Kirkpatrick, Neil J. Holbrook and Nathan L. Bindoff (*Bull. Amer. Meteor. Soc.*, **99** (1), S44–S48) • ©2017 American Meteorological Society • DOI:10.1175/BAMS-D-17-0093.2

Supplementary methods.

The NINO34 index (Trenberth 1997) was calculated by spatially averaging SST anomalies over (5°S–5°N, 170°–120°W), and filtering the result with a 3-year running average. The dipole mode index (DMI; Saji et al. 1999) was calculated by spatially averaging SST anomalies over a west box (10°S–10°N, 50°–70°E), an east box (10°–0°S, 90°–100°E), differencing (west minus east), and filtering the result with 1-year running average. The tripole mode index (TMI; Henley et al. 2015) was estimated by first spatially averaging SST anomalies over a north box (24°–45°N, 140°E–145°W), a south box (50°–15°S, 150°E–160°W), and an equatorial box (10°S–10°N, 170°E–90°W), and then calculating the index as "equatorial box – 0.5 × (north box + south box)" and filtering with 10-year running average. All indices were standardized to have zero mean and unit variance. Note that to preserve adequate ensemble size no model selection has taken place, and so results could be sensitive to the model representation of these modes. The models represent reasonably well the expectations from observations of the three climate modes (e.g., Deser et al. 2010), with the exception of CNRM-CM5 (Fig. ES9.2). Note that the interdecadal Pacific oscillation, as represented here by the TPI, is strongly correlated with the Pacific decadal oscillation ($r = 0.83$; Henley et al. 2015). These two modes are not independent of one another and both are associated with temperature anomalies in the far North Pacific.

REFERENCES

Deser, C., M. A. Alexander, S. P. Xie, and A. S. Phillips, 2010: Sea surface temperature variability: Patterns and mechanisms. *Annu. Rev. Mar. Sci.*, **2**, 115–143, doi:10.1146/annurev-marine-120408-151453.

Henley, B. J., J. Gergis, D. J. Karoly, S. Power, J. Kennedy, and C. K. Folland, 2015: A tripole index for the Interdecadal Pacific Oscillation. *Climate Dyn.*, **45**, 3077–3090, doi:10.1007/s00382-015-2525-1

Saji, N. H., B. N. Goxwami, P. N. Vinayachandran, and T. Yamagata, 1999: A dipole mode in the tropical Indian Ocean. *Nature*, **401**, 360–363.

Trenberth, K. E., 1997: The definition of El Niño. *Bull. Amer. Meteor. Soc.*, **78**, 2771–2777, doi:10.1175/1520-0477(1997)078<2771:TDOENO>2.0.CO;2.

Table ES9.1. CMIP5 models used in the event attribution analysis. The number of ensemble members for each model experiment is listed for each model, along with the bias correction applied to the non-seasonal standard deviation of the model SST time series for NA and BSGA (positive values indicates the model variability was increased by the correction). These were the only models with daily sea surface temperatures available.

Model	Historical	Historical-Nat	RCP8.5	Bias correction (NA)	Bias correction (BSGA)
ACCESS1.3	3	3	1	1.69	1.06
CanESM2	1	3	5	1.70	0.71
CSIRO Mk3.6.0	10	10	10	1.24	0.82
CNRM-CM5	1	5	5	1.12	1.28
HadGEM2-ES	4	4	4	1.54	0.95
IPSL-CM5A-LR	6	3	4	1.40	0.66
IPSL-CM5A-MR	3	3	1	1.44	0.76
Total	**28**	**31**	**30**	—	—

Table ES9.2. Role of climate modes in modulating MHW properties and frequency. For intensity and duration, if the probability distributions of these properties are significantly different from each other between the positive and negative phases of the modes ($p < 0.01$) then the 90th percentiles of these metrics are indicated, otherwise the cell contains a '—' ($p > 0.01$). For frequency, if the 99% confidence intervals of event occurrence between the positive and negative phases of each mode overlap then the cell contains a '—' ($p > 0.01$), otherwise the mode has a significant impact on MHW frequency ($p < 0.01$) and the median frequency in that phase is shown.

Mode		Northern Australia			Bering Sea / Gulf of Alaska		
Index	**Phase**	**Intensity**	**Duration**	**Frequency**	**Intensity**	**Duration**	**Frequency**
NINO34	Positive	—	—	—	—	86 days	41.8%
	Negative	—	—	—	—	59 days	19.3%
DMI	Positive	1.04°C	40 days	15.4%	1.39°C	—	37.3%
	Negative	0.99°C	74 days	46.0%	1.32°C	—	27.4%
TPI	Positive	—	—	—	—	85 days	39.3%
	Negative	—	—	—	—	65 days	23.3%

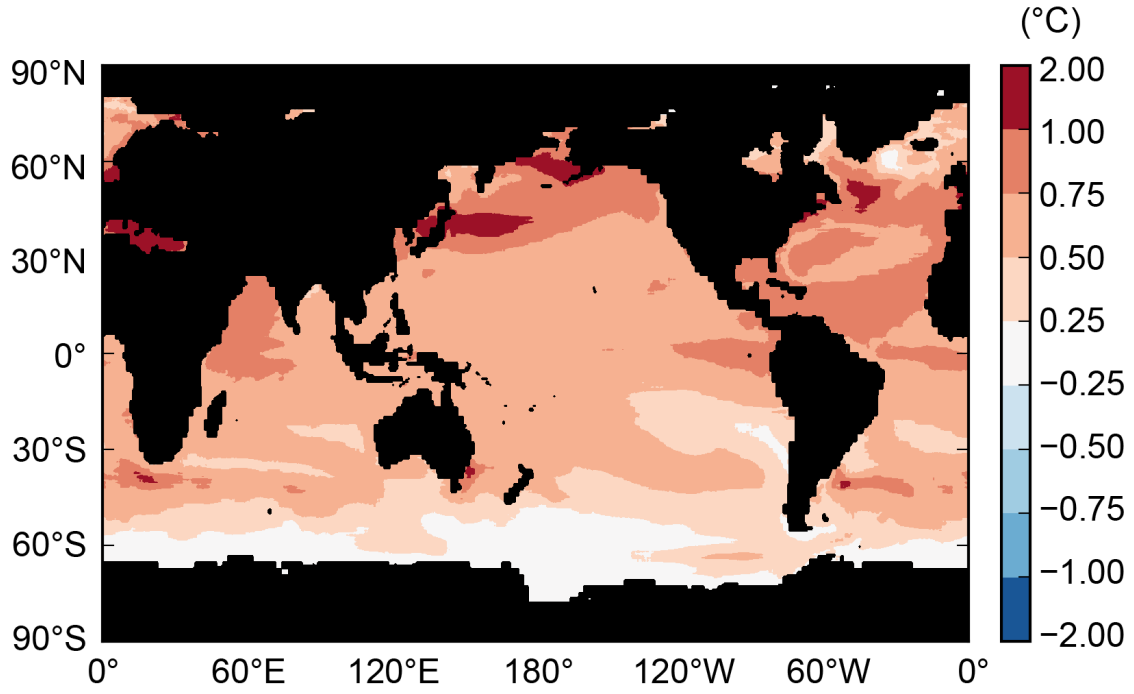

Fig. ES9.1. Global pattern of anthropogenic warming. Colors indicate the difference between the multimodel mean estimates of mean SST (°C) during 2006–20 from the RCP8.5 simulations and 1961–90 from the historical simulations.

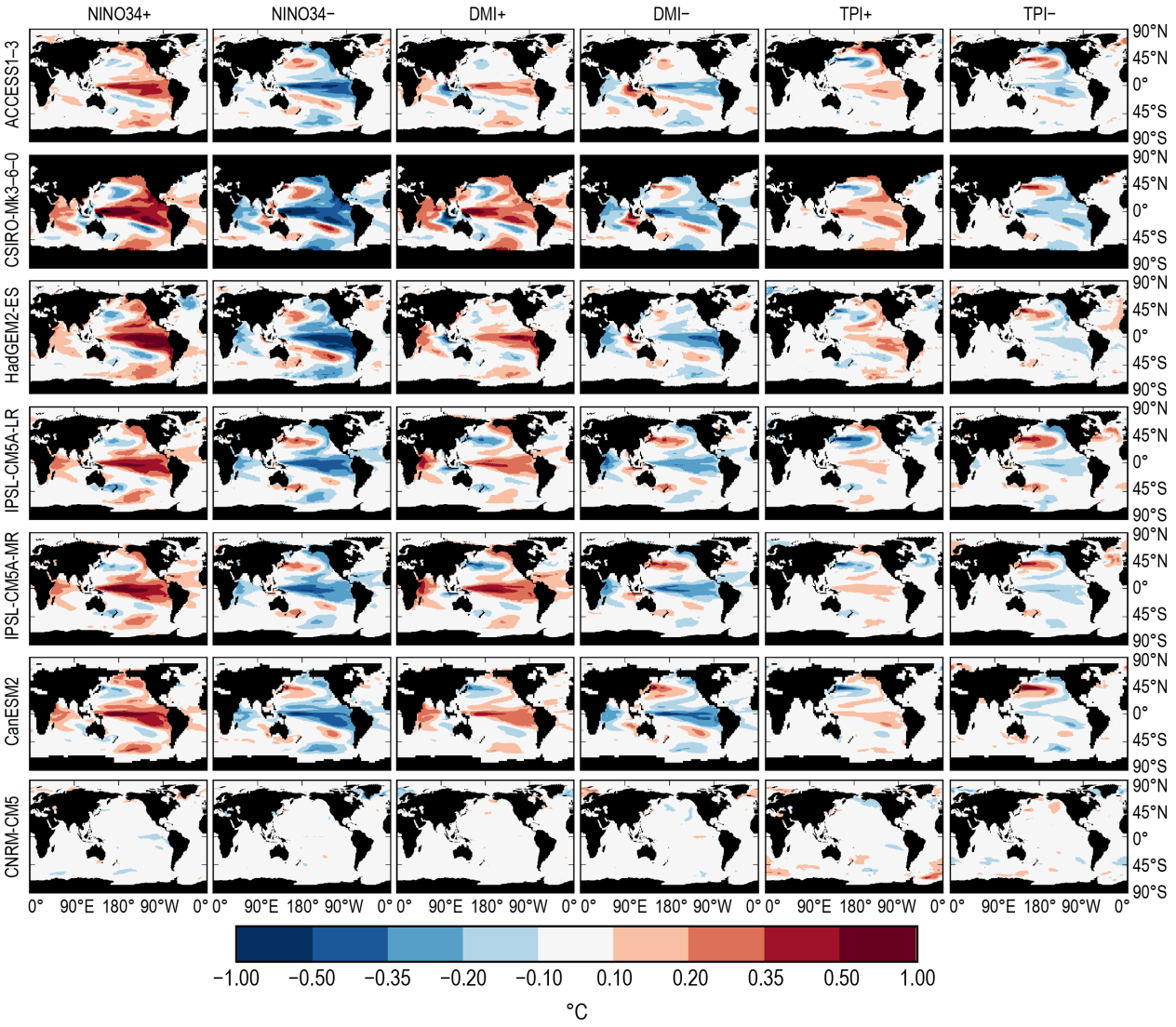

Fig. ES9.2. Modes of climate variability as represented by the CMIP5 global climate models. Each panel shows the composite average of model temperature anomalies (°C) during the positive and negative phases of the three climate mode indices considered (NINO34, DMI, TPI; columns). Individual models are presented as separate rows.